Human microbiome-derived peptide affects the development of experimental autoimmune encephalomyelitis via molecular mimicry

Authors

Xin Ma[1, #], Jian Zhang[2, #], Qianling Jiang[1], Yong-Xin Li[2, *] and Guan Yang[1,3 *]

Affiliations

1. Department of Infectious Diseases and Public Health, Jockey Club College of Veterinary Medicine and Life Sciences, City University of Hong Kong, Kowloon, Hong Kong SAR, China.

2. Department of Chemistry and The Swire Institute of Marine Science, The University of Hong Kong, Pokfulam Road, Hong Kong SAR, China.

3. Shenzhen Research Institute, City University of Hong Kong, Shenzhen, China

#equal contribution

*Corresponding Authors: Yong-Xin Li, Guan Yang.

Email: yxpli@hku.hk, gyang25@cityu.edu.hk

Summary

Background: Gut commensal microbiota has been identified as a potential environmental risk factor for multiple sclerosis (MS), and numerous studies have linked the commensal microorganism with the onset of MS. However, little is known about the mechanisms underlying the gut microbiome and host-immune system interaction.

Methods: We employed bioinformatics methodologies to identify human microbial-derived peptides by analyzing their similarity to the MHC II-TCR binding patterns of self-antigens. Subsequently, we conducted a range of *in vitro* and *in vivo* assays to assess the encephalitogenic potential of these microbial-derived peptides.

Findings: We analyzed 304,246 human microbiome genomes and 103 metagenomes collected from the MS cohort and identified 731 nonredundant analogs of myelin oligodendrocyte glycoprotein peptide 35-55 (MOG_{35-55}). Of note, half of these analogs could bind to MHC II and interact with TCR through structural modeling of the interaction using fine-tuned AlphaFold. Among the 8 selected peptides, the peptide (P3) shows the ability to activate MOG_{35-55}-specific $CD4^+$ T cells *in vitro.* Furthermore, P3 shows encephalitogenic capacity and has the potential to induce EAE in some animals. Notably, mice immunized with a combination of P3 and MOG_{35-55} develop severe EAE. Additionally, dendritic cells could process and present P3 to MOG-specific $CD4^+$ T cells and activate these cells.

Interpretation: Our data suggests the potential involvement of a MOG_{35-55}-mimic peptide derived from the gut microbiota as a molecular trigger of EAE pathogenesis. Our findings offer direct evidence of how microbes can initiate the development of EAE, suggesting a potential microbiome-based therapeutic target for inhibiting the progression of MS.

Funding: National Natural Science Foundation of China (82371350 to GY)

Keywords: multiple sclerosis, experimental autoimmune encephalomyelitis, molecular mimicry, gut microbiota

Research in context

Evidence before this study

On July 31, 2024, we conducted a search on PubMed for articles containing the phrases "gut microbiome and multiple sclerosis" and "gut microbiome and experimental autoimmune encephalomyelitis." This search yielded a total of 630 and 151 articles, respectively, indicating that the relationship between gut microbiota and the development of MS and EAE is well established. In contrast, our search for "gut microbiome and molecular mimicry and experimental autoimmune encephalomyelitis" revealed only two review papers, highlighting a significant gap in the literature regarding the role of molecular mimicry in connecting gut microbiome dynamics to the development of EAE.

Added value of this study:

In this study, we employed bioinformatics tools to screen for microbial-derived peptides in the gut that potentially cross-react with autoantigen-specific TCR. Our key findings include: 1) Identification of MOG_{35-55} mimics within the human gut microbiome by employing a combination of TCR-binding footprint screening and prediction model of peptide-MHC II-TCR complexes; 2) Microbial-derived MOG_{35-55} mimics can cross-react with MOG_{35-55}-specific $CD4^+$ T cells; 3) Among them, peptide 3 predicted from *Akkermansia muciniphila* can induce moderate EAE in mice; 4) Dendritic cells could process and present peptide 3 to MOG-specific $CD4^+$ T cells and activate these cells.

Implications of all the available evidence:

This study suggests the potential involvement of a MOG_{35-55}-mimic peptide derived from the gut microbiota as a molecular trigger of EAE pathogenesis. These data may provide a potential microbiome-based therapeutic target for inhibiting the progression of MS.

Introduction

Multiple sclerosis (MS) is an autoimmune disease characterized by the involvement of autoreactive T cells targeting myelin antigens, leading to the destruction of myelin and damage to axons, resulting in neurologic syndromes and physical disability (1). The global prevalence of MS stands at approximately 2.8 million individuals (2), with an increasing incidence observed in developing countries and among children (3). Although the etiology of MS remains unknown, both genetic and environmental factors have been implicated in its development (1). Accumulating evidence suggests that gut microorganisms play a pathogenic role in MS (4, 5). Research has found notable differences in the composition of gut bacteria between MS patients and healthy individuals (6, 7). Similar alterations in the gut microbiota, including elevated levels of *Akkermansia muciniphila* (*A. muciniphila*), have also been observed in experimental autoimmune encephalomyelitis (EAE), an animal model employed to investigate MS (8). However, how the alterations in the gut microbiota might affect MS/EAE development remains largely unknown.

Molecular mimicry is one of the leading mechanisms in linking the role of microbiota in immune reactivity in autoimmune diseases and cancer (9-13). Reassuringly, it has been reported that microbiota-derived peptides resembling myelin basic protein (MBP) can activate autoreactive T cells in MS (14-16). MBP, along with proteolipid protein and myelin oligodendrocyte glycoprotein (MOG), are myelin antigens targeted by HLA-DR-restricted T cells, leading to MS development (1). Prior studies have demonstrated that hepatitis B virus polymerase can partially mimic MBP, leading to mononuclear cell infiltration in the central nervous systems (CNS) of animals immunized with selected peptide from this viral protein (17). Of note, MOG has been considered a primary target of cellular and humoral immune responses in multiple diseases due to its special extracellular immunoglobulin domain, which is directly accessible to binding partners including antibodies (18-20). Furthermore, the MOG_{35-55} peptide has been widely used to induce EAE. Intrigued by these findings, we hypothesized that microbiome-derived peptides resembling the MOG_{35-55} epitope could trigger the autoimmune response responsible for initiating EAE.

To address this hypothesis, we analyzed human microbiome genomes and metagenome databases collected from the MS cohort. We aimed to identify microbial peptides with MHC II-TCR recognition patterns resembling those of MOG_{35-55}, which is presented by the MHC class II I-A^b and induces chronic EAE in C57BL/6J mice (21). Subsequently, we identified, synthesized, and tested 8 of these peptides for their ability to activate MOG_{35-55}-specific T cells. Our findings revealed that a predicted peptide (P3) derived from the gut commensal organism *A. muciniphila* can activate mouse MOG_{35-55}-specific T cells *in vitro*, albeit to a lesser extent compared to the MOG_{35-55} peptide. Furthermore, P3 shows encephalitogenic capacity and has the potential to induce EAE in some animals. Notably, we found

that mice immunized with a combination of P3 and MOG_{35-55} developed more severe EAE. Additionally, dendritic cells (DCs) were able to process P3 and present it to $CD4^+$ T cells isolated from 2D2 mice expressing a MOG-specific T cell receptor. Our findings suggest that microbial peptide derived from the gut commensal, resembling MOG_{35-55}, may mimic the native myelin peptide and potentially contribute to EAE development.

Material and Methods

Identify the human MOG_{35-55} peptide analog in the human microbiome genomes and human-associated metagenomic samples

We first collected and curated human microbiome-derived peptide resources, which included human microbiome genomes and human-associated metagenomics samples. In detail, we collected 286,997 human microbiome genomes from Unified Human Gastrointestinal Genome dataset (UHGG, v1.0) (22), and 17249 genomes from CIBIO species-level genome bins (23). Taxonomic assignments were performed for genomes from CIBIO by GTDB-tk (24). In addition, we downloaded 103 metagenomes from MS patients in National Bioscience Database Center (NBDC) Human Database with the accession number of hum0197 (25). The data obtained from the UHGG and NBDC were acquired in accordance with human research ethics guidelines and were approved by the Human Ethics sub-Committee of the City University of Hong Kong (jcc2223ay001). For these metagenomic samples, we applied metagenomic assembly to obtain contigs using MEGAHIT (26) for each sample separately. Taxonomic classification was further conducted for the resulting contigs using CAT (v5.2.3) (27). Taxonomic assignments for genomes or contigs based on the Genome Taxonomy Database (28). Finally, all open reading frames were predicted in each genome or contig using Prodigal-short (29). Human MOG_{35-55} sequence analog searching was conducted by BLASTp with an e-value threshold of 0.001 in a pool of proteins from the above Human microbiome-derived peptide resources.

The structure-based prediction of peptide-MHC II-TCR binding

Identified analogs were first filtered based on whether they contained the motifs with [YR..F.RV.], [YR..F.R..], [YR..F..V.], [YR....RV], and [Y...F.RV.] are involved in the peptide-MHC-TCR interactions. Next, a special peptide region (~ 21 residues) containing the above binding pattern was truncated from these filtered analogs. The yielded nonredundant truncated peptides were subjected to further analyses.

The peptide-MHC II-TCR binding prediction was performed in two steps: the peptide-MHC II binding specificity prediction and TCR: peptide-MHC II interactions modeling. Because the advanced peptide-MHC II structure prediction tools often predict the binding structure composed by the binding core of peptides (normally with 9 residues) and receptors (MHC II or TCR) (30-34), these nonredundant

truncated peptides were further chopped into a series of consecutive 11-residue windows along peptide with the putative core nine-mer residues and their immediate neighboring residues. The resulting 11-residue windows were subjected to a fine-tuned AlphaFold (35) to predict peptide-MHC II binding with the following parameters: --model_names model_2_ptm_ft --ignore_identities (30). Peptide-MHC II templates (4p23_MH2_H2ABa_H2ABb.pdb,6mng_MH2_H2ABa_H2ABb.pdb,1muj_MH2_H2ABa_H2ABb.pdb) in the PDB template set were used (30). Mean Inter-chain lowest predicted aligned error (PAE) terms corresponding to the peptide-MHC interactions ≤ 4.34 and peptides' per-residue confidence score (pLDDT) corresponding to local structural accuracy ≥ 90 were used to classify MHC II binder and non-binder. Next, peptide-MHC II-TCR binding for the predicted binders was modeled by a specialized version of the neural network predictor AlphaFold and TCR–pMHC complex templates-based method, TCRDock with 'model_2_ptm' and '--benchmark' parameter set (32). Based on TCRDock's workflow, three simulations were conducted for each target peptide-MHC II-TCR complex and finally chose the model with the lowest PAE between the TCR and pMHC. Given the hypervariable gene segments in TCR alpha and beta chain largely determine the structure modeling (36), we took TCR:pMHC II structural templates (PDB IDs: 3c60, 3rdt, 3c5z, 6mnn), pairing with four types of mouse TCR, to model the peptide-MHC II-TCR structures. The predicted structures were visualized by PyMoL (Version 2.5.3).

Mice used in this Study

Six to eight-week-old C57BL/6J (RRID: MGI: 2159769) mice were obtained from the Laboratory Animal Research Unit (LARU) of City University of Hong Kong. The 2D2 TCR transgenic mice C57BL/6-Tg (Tcra2D2, Tcrb2D2) 1Kuch/J (RRID: IMSR_JAX: 006912) were purchased from The Jackson Laboratory and bred in LARU. Mice were housed under a 12-hour light/dark cycle in individually ventilated cages. Food and water were provided ad libitum throughout the study.

Ethics

All experimental procedures were approved by the Animal Ethics Committee of the City University of Hong Kong (approval number AN-STA-00000493) and performed in accordance with LARU Guidelines.

Reagents and resources

Reagents and resources are summarized in Supplementary Table 1.

Active EAE induction

For induction of active EAE, six to eight-week-old mice of both sexes were immunized subcutaneously at two sites on the back flank area with 200 µg of P3 (TTLSFYRPPFLRVRRPFYIIF) or $MOG_{35–55}$ (MEVGWYRSPFSRVVHLYRNGK)

peptide (Thermo Fisher, J66557.MCR) emulsified in 200 µl incomplete Freund's adjuvant (BD bioscience, 263910) supplemented with 2 mg/ml heat-killed *Mycobacterium tuberculosis* (BD bioscience, 231141). Mice then received intraperitoneal 400 ng of pertussis toxin (Calbiochem, 516561) at 0- and 2-day post-immunization (dpi). To check if P3 could aggravate classic EAE, mice were immunized with either the combination of P3 and $MOG_{35–55}$ (200 µg P3 + 50 µg $MOG_{35–55}$), MOG_{35-55} (50 µg), or the combination of a scrambled peptide (KGNRYLHVVRSFPSRYWGVEM) and $MOG_{35–55}$ (200 µg scrambled peptide + 50 µg $MOG_{35–55}$). Priori calculation was not performed, and sample sizes were determined from prior preclinical studies. EAE severity was scored daily in a blinded manner across all groups using the standard scale: 0, no disease; 0.5, tail tip limp; 1, loss of tail tone; 1.5, one leg shows weakness; 2, both legs show weakness with some movement; 2.5, one leg is limp; 3, hind limb paralysis; 3.5, hind limb paralysis and limited movement of waist; 4, hind limb paralysis and forelimb weakness; 4.5, both hind limb and forelimb paralysis; 5, moribund/death (37).

Antigen recall assay

The peripheral T cell antigen recall response was performed in splenocytes collected from EAE mice at 10 dpi. Mice were anesthetized by 3% isoflurane inhalation and then euthanized by cervical dislocation. Spleens were then collected from the euthanized mice and crushed through a 70-µm cell strainer and centrifuged at 400 × g for 5 min at 4 °C, then incubated in red blood cell lysis buffer (Thermo Fisher, A1049201) for 5 min. After centrifuge, isolated cells were plated at a density of $5x10^5$ cells/well and stimulated with synthesized peptide or $MOG_{35–55}$ (20 µg/ml final concentrations) in RPMI 1640 complete medium (RPMI1640 (Thermo Fisher, 11875093), 10% FBS (Thermo Fisher, A5256801), 2 mM L-glutamine (Thermo Fisher, A2916801), 10 mM Hepes (Thermo Fisher, 15630130), 50 µM 2-mercaptoethanol (Sigma-Aldrich, M6250), 100 IU penicillin (Solarbio, A8180), and 100 µg/mL streptomycin (Solarbio, S8290)), in a total volume of 200 µL per well. Cells were stimulated for 18-hour at 37 °C and 5% CO_2 atmosphere as previously described (38), then analyzed by flow cytometry for cytokine (IFN-γ, IL-17A) producing cells. To check the antigen recall response of the CNS-infiltrated T cell, spinal cord was collected after euthanizing mice on 17 dpi. Spinal cord tissues were minced and incubated in RPMI 1640 supplemented with 2% FBS, 400 U/ml collagenase IV (Thermo Fisher, 17104019), and 20 µg/ml DNase I (Thermo Fisher, 18047019) for 45 min at 37 °C with agitation. The digested tissues were filtered through a 70-µm filter, and the myelin debris were removed by resuspending the pellet after centrifuge in 40% Percoll (Cytiva, 17089109) and overlaid onto 70% Percoll followed by centrifugation at 860xg for 20 min at 20 °C. Leukocytes at the interface were collected.

Passive EAE induction

Spleens were collected from mice immunized with MOG_{35-55} at 10 dpi. Splenocytes were restimulated with either MOG_{35-55} or P3 (50 μg/ml) and incubated in RPMI 1640 complete medium at a concentration of 5×10^6 cells/ml with the presence of IL-12 (2 ng/ml) for 72 h at 37 °C. Cells were then collected and resuspended in PBS. A total of 2×10^7 stimulated cells were intraperitoneally injected into C57B/L6J recipients. The clinical scores were graded similarly to active EAE.

Histopathology

Inflammation and demyelination of spinal cords were assessed on day 17 after immunization. The lumbar enlargement of the spinal cords was isolated from animals and instantly fixed in 4% paraformaldehyde for a minimum of 48 h, then embedded in paraffin and sectioned at 5-μm thickness. Sections were stained with H&E (Solarbio, G1120) or LFB (Abcam, ab150675) to evaluate inflammation and demyelination. The sections were scanned using a NanoZoomer S60 Digital slide scanner (Hamamatsu, C13210-01). The degrees of inflammation (H&E scores) were calculated as 0, normal; The severity of demyelination (LFB scores) was analyzed as 0, normal; 1, myelin sheath injuries in rare areas; 2, a few areas of demyelination; 3, confluent perivascular or subpial demyelination; 4, massive demyelination involving one half of the spinal cord; and 5, extensive demyelination involving the whole spinal cord (39).

Antigen presentation assays

To obtain stimulator DCs, single cell suspensions from the spleen collected from C57BL/6J mice were prepared by mechanical disruption on a 70-μm cell strainer. Cell suspensions were resuspended in MACS buffer (0.5% BSA (Beyotime, ST025), 2 mM EDTA (Solarbio, E8040) in PBS) after lysing red blood cells. $CD11c^+$ cells were then negatively selected according to the manufacturer's instructions using the mouse Pan Dendritic Cell Isolation Kit (Miltenyitec, 130-100-875). Isolated DCs were pulsed with either PBS, P3, or MOG_{35-55} at 20 μg/ml final concentrations, using 2×10^4 cells in a 96-well plate for 1 h at 37 °C. Cells were then washed extensively and used for co-culture with responder 2D2 $CD4^+$ T cells. Responder MOG_{35-55}-specific $CD4^+$ T cells were isolated from 2D2 TCR transgenic mice spleen by using $CD4^+$ T cells Isolation Kit (Miltenyitec, 130-104-454). Sorted $CD4^+$ T cells were labeled with Carboxyfluorescein succinimidyl ester (CFSE, Thermo Fisher, C1157) following the user guide. A total of 10^5 CFSE labeled 2D2 $CD4^+$ T cells were then seeded in triplicate in a round bottom 96-well plate with 2×10^4 stimulated DCs (5:1 ratio). DCs and T cells were cultured together for 72-hour at 37 °C and 5% CO_2 atmosphere, then cells were prepared for flow cytometry to detect T cell proliferation and RNA from these cells was collected for checking *Il17a* and *Ifng* mRNA expression level by RT-qPCR.

Evaluation of DC activation

To determine the activation state of DCs, isolated DCs were primed with either MOG_{35-55}, P3, or scrambled peptide (20 μg/ml) for 1 h at 37 °C, followed by culturing these cells in RPMI 1640 complete medium at a concentration of 2×10^5 cells/ml. The cultured DCs were then harvested at different time points after priming and examined for the activation state by checking the expression levels of CD80, CD86, and MHC II using flow cytometry.

Gene expression analysis by reverse transcription–qPCR (RT-qPCR)

The total RNA of cells was extracted using RNAiso Plus (Takara, 9108) and reverse-transcribed into cDNA using HiScript III All-in-one RT SuperMix (Vazyme, R333-01) according to the manufacturer's protocol. qPCR was performed using Taq Pro Universal SYBR qPCR Master Mix (Vazyme, Q712) on a QuantStudio 7 Pro Dx Real-Time PCR System (Thermo Fisher). Primer sequences are listed in Supplementary Table 2 and were synthesized by Tsingke Biotech. The results are shown as relative expression values normalized to *Gapdh*.

Flow cytometry

Single cell suspensions from the spleen were obtained by mechanical disruption on a 70-μm cell strainer, then incubated in red blood cell lysis buffer for 5 min. For the staining process, dead cells were stained with Propidium Iodide (Sigma-Aldrich, 537060) or Live/Dead Ghost dye (Tonbo Biosciences, 13-0870-T100). For staining of surface markers, cells were incubated in fluorescently labeled antibodies (CD45 (Biolegend, 103132), CD3 (Biolegend, 100235), CD4 (Biolegend, 100437), CD69 (Biolegend, 104513), TCR $V_{\beta}11$ (Biolegend, 139003), CD11C (Biolegend, 117307), CD80 (Biolegend, 104725), CD86 (Biolegend, 105039), MHC II (Biolegend, 107628)) for 30 min in FACS buffer (PBS containing 2% FBS) at 4 °C. For intracellular staining, cells were washed with 2 mL wash buffer, then fixed and permeabilized by using Cytofix/Cytoperm™ Fixation/Permeabilization Kit (BD Biosciences, 554714) as manufacturer's instructions. Fixed cells were incubated in fluorescently labeled antibodies (IFN-γ (Biolegend, 505849), IL-17A (eBioscience™, 25-7177-82)) for 30 min in permeabilization buffer at 4 °C. All data were collected on a BD Celesta flow cytometer (BD Biosciences) and analyzed using FlowJo software (v.10.2, BD Biosciences).

Statistical analysis

Data were analyzed using GraphPad Prism software (Version 9.5.1) and reported as mean ± SEM unless otherwise noted. Gaussian distributions were verified with the Kolmogorov-Smirnov test. The two-tailed unpaired Student *t-test* was used for determining differences between two groups with equal variances, whereas Welch's t-test was employed for groups with unequal variances. The statistical differences between more than two groups were analyzed using one-way ANOVA with Tukey's post-test for multiple comparisons. A Mann–Whitney *U* test was used to assess the

significance of EAE clinical scores throughout the disease course. For groups with 3 biological replicates, we used the nonparametric Wilcoxon test for two-group comparisons and one-way nonparametric ANOVA for more than two groups' comparisons. Statistical significance was defined as a *p*-value < 0.05.

Role of Funders

Funders had no role in study design, data collection, data analyses, interpretation, and writing of the manuscript, or the decision to publish the results.

Results

Well-defined peptide-MHC II-TCR binding motifs guided microbiome-derived epitope discovery from the human microbiome

To uncover the microbiome-derived epitopes resembling the immunodominant MOG_{35-55} peptide, we designed a genome mining workflow involving an analysis of a vast dataset comprising 304,246 human microbiome genomes (23, 40) and 103 metagenomic samples from an MS study cohort (41) (Fig 1A). We first extracted 404,181 MOG_{35-55} analogs (Supplementary Table 3) from these resources, followed by a filtering process that retained 21,557 analogs (3,946 non-redundant sequences) possessing well-defined binding residues at specific sequential spacing (Fig 1B, Supplementary Table 4).

To gain insight into the phylogenetic distribution of MOG_{35-55} analogs derived from the human microbiome, we examined the 21,557 analogs with well-defined binding motifs. Those analogs exhibited a wide distribution across 24 phyla, with the occurrence of a specific motif per genome varying from 0 to 1 within each phylum (Fig 1C). Of note, 10 phyla with fewer than 10 genomes and 19 unclassified bacteria-derived contigs at the phylum level were grouped as "Others". Interestingly, Verrucomicrobiota demonstrated a higher likelihood of encoding analogs featuring the YRxxFxRVx motif. Besides, these analogs were predominantly encoded by species such as *A. muciniphila* or *A. muciniphila.B*, which are enriched in patients with MS (42).

Microbiome-derived peptide-MHC II-TCR complexes structure-prediction

Following the general model of antigen presentation (43, 44), we employed a fine-tuned AlphaFold with a binding classifier (30) to discriminate ligands with mouse MHC II molecules (H2-Ab) binding core peptides. Subsequently, the binding core peptides were subjected to modeling the peptide-MHC II-TCR complex by TCRdock (32). First, the performance of fine-tuned AlphaFold and TCRdock was assessed using the MOG_{35-55} peptide as a test case (Fig 2). MOG_{35-55} peptide was further chopped into 10 unique putative binding core peptide candidates (Fig 2A) for subsequent analyses. This was necessary because the current state-of-the-art machine learning-based structure predictors (30, 32-34) for the peptide-MHC II-TCR

complex are designed to predict binding between a 9-mer binding core peptide and its receptor (MHC II or TCR). Finally, the binding core peptide of MOG_{35-55}, with the specific sequence "WYRPPFSRVVH", was predicted to be MHC II binders (Fig 2A), and this binding core peptide exhibited reliable interactions with four TCRs that contained different gene segments (Fig 2B). It is noteworthy that this binding core peptide of MOG_{35-55} could interact with mouse MHC II-TCR complex in our pMHC II-TCR model with observed hydrogen bonds (Fig 2C and 2D), which is consistent with the previous studies (21, 45). Inspired by these results, we integrated these two methods to prioritize the microbiome-derived epitopes.

To mimic the process of proteolytical degradation of exogenous proteins before their presentation to MHC II in antigen presentation (44), we truncated the corresponding peptide windows (~ 21 residues) containing the binding motifs along these 3,946 analogs, resulting in 731 nonredundant putative ligand sequences (Fig 3A, Supplementary table 4, 5). These ligands were further chopped into 5,783 unique putative binding core peptide candidates (Supplementary Table 5) for subsequent analyses. Consequently, we identified 493 binding core peptides from 439 ligands as MHC II binders (Fig 3B, Supplementary Table 6). In addition, we successfully modeled interactions between peptide-MHC II and 4 types of TCRs for 97.8% of the MHC II binders using 4 peptide-MHC-TCR complexes templates (Supplementary Fig 1 and Fig 2, Supplementary Table 6). To determine the binding specificity, binding motifs are generated from these binding core peptides and characterized by anchor positions (Fig 3C and 3D). The motifs revealed that Y/F, R, F, R, and V residues are enriched at well-defined anchor positions (loc_1, loc_2, loc_5, loc_7, loc_8) in this study. Surprisingly, several noncanonical binding motifs starting with “L”, “A”, “I”, “S”, “N”, “H”, “Q”, “V”, “T”, “M”, “W”, and others were also observed (Fig 3C). These findings suggest that microbiome-derived epitopes could interact with MHC II and TCRs with diverse binding characteristics.

Microbiome-derived peptide stimulates MOG_{35-55}-specific T cell

To investigate the potential modulatory effects of microbiome-derived peptides resembling MOG_{35-55} peptide sequence on the autoimmune response that triggers EAE, a total of 8 peptides (Fig 3 and 4A) were selected from a pool of 439 ligands. These 8 peptides were confidently modeled in pMHC II-TCR interactions (Fig 3), and their selection was based on four specific criteria. Firstly, ligands that contained the "YRxxFxRVx" motif were considered. Secondly, ligands that could be detected in the NBDC database were included (specifically, P1, P2, P4, P5, P6, and P8). Thirdly, ligands collected from species related to MS were chosen (P3 and P5) (42). Finally, ligands containing noncanonical binding motifs starting with "F" and "L" were selected (P1, P3, P7, and P8), as these motifs were found to be most enriched in the pool of 493 binding core peptides. To investigate the potential of microbe-derived peptides to activate MOG_{35-55}-specific T cell, we stimulated splenocytes

isolated from MOG_{35-55}-induced EAE mice with MOG_{35-55} peptide and 8 selected peptides (Fig 4A). Of the tested 8 microbiome-derived peptides, P3 demonstrated the capacity to stimulate the production of IL-17 and IFN-γ by peripheral MOG_{35-55}-specific T cells from spleen that were isolated from mice at 10 dpi (Fig 4B-4D, Supplementary fig 3A). Furthermore, P3 also stimulated the production of IFN-γ and IL-17 by spinal cord-infiltrated $CD4^+$ T cells during the peak phase of EAE (Fig 4E and 4F). It is noteworthy that P3 was identified as originating from *A. muciniphila*, a gut commensal that is significantly enriched in the gut microbiota of individuals with MS (5).

P3 shows encephalitogenic capacity *in vivo*

To further explore the encephalitogenic potential of the P3, we immunized the C57BL/6J mice with P3 (Fig 5A). We found that P3 could induce EAE development in some mice, although both clinical score and incidence were low (disease incidence = 2/12, Fig 5B and 5C). We further stimulated splenocytes from P3-immunized mice sacrificed at 10 dpi with either P3 or MOG_{35-55} for 18-hour (Supplementary fig 4A). Following stimulation, the cells exhibited a robust immune response to P3 and a relatively weaker response to MOG_{35-55} as indicated by the production of IFN-γ (Supplementary fig 4B-4D), suggesting that MOG_{35-55} can cross-react with P3-specific T cells.

To directly assess the encephalitogenic capacity of P3, we collected splenocytes from MOG_{35-55} immunized mice at 10 dpi and restimulated them with P3. These activated cells were then adoptively transferred to C57BL/6J recipients to induce passive EAE (Fig 5D). As shown in Fig 5E and 5F, recipient mice that received P3-stimulated splenocytes developed EAE with weak symptoms and low incidence. Although the symptoms and incidence were modest, these results suggest that P3 possesses the encephalitogenic capacity.

P3 in combination with MOG_{35-55} exacerbates EAE development in mice

To further explore the impact of P3 on classic EAE development, C57BL/6J mice were immunized with a combination of P3 and a low dose of MOG_{35-55} (Fig 6A). We found that P3 in combination with MOG_{35-55} could exacerbate EAE development in mice (Fig 6B). To determine the difference of the immune responses in the peripheral between these two groups, we stimulated splenocytes from mice immunized with P3 + MOG_{35-55} or scrambled peptide + MOG_{35-55} with MOG_{35-55}. We found that MOG_{35-55} could induce higher levels of IL-17 and IFN-γ in splenocytes collected from mice immunized with P3 + MOG_{35-55} (Fig 6C). At 17 dpi, the spinal cord tissues were collected, and flow cytometry as well as Hematoxylin and Eosin (H&E) or Luxol Fast Blue (LFB) staining were performed to determine the impact of P3 on the severity of inflammation and demyelination. Mice immunized with P3 + MOG_{35-55} displayed more severe inflammation and increased demyelination in the

white matter of the spinal cord compared to the other group, with the P3 + MOG_{35-55} group showing significantly higher inflammatory scores (H&E score) and a rising trend in demyelination levels (LFB score) than the Scrambled peptide + MOG_{35-55} group (Fig 6E and 6F). These higher inflammatory scores and demyelination levels in the P3 + MOG_{35-55} group are associated with increased leukocyte infiltration (Fig 6D, Supplementary fig 3B, Supplementary fig 5). We also checked if immunization of P3 could affect the recovery phase of EAE and found that the combination of P3 and MOG_{35-55} showed no significance on the recovery of EAE (Supplementary fig 6A and 6B).

DCs process microbiome-derived peptide P3 and further activate 2D2 $CD4^+$ T cell proliferation

Given that P3 stimulated MOG_{35-55}-specific $CD4^+$ T cells *in vitro*, we investigated whether DCs are capable of processing and presenting P3 to MOG_{35-55}-specific T cells. Our pMHC II-TCR model predicted an interaction between the core 9-mer residues truncated from P3 and the MHC II-TCR complex (Fig 7A and 7B). Hydrogen bonds were observed inside the recognition model similar to the docking result from MHCII-MOG_{35-55}-TCR complex (Fig 2C and 2D), leading us to hypothesize that this peptide could be presented by DCs. To test this hypothesis, we performed an antigen presentation assay using DCs isolated from the spleens of C57BL/6J mice. The DCs were primed with either PBS, P3, or MOG_{35-55}, and then co-cultured with sorted 2D2 $CD4^+$ T cells. The activation status of $CD4^+$ T cells was later assessed by quantifying the expression of the early T cell activation marker CD69. Furthermore, the proliferation of $CD4^+$ T cells was evaluated by monitoring the changes in the population of CFSE-labeled cells. The results demonstrated that P3 could be presented by DCs and subsequently activate the proliferation of 2D2 $CD4^+$ T cells (Fig 7C, Supplementary fig 3C). However, P3 induces a weaker $CD4^+$ T cell activation and proliferation than MOG_{35-55} (Fig 7D), which may explain the lower incidence and clinical score observed in P3-induced EAE (Fig 5B and 5C). Furthermore, we noticed that co-culturing P3 with DCs and 2D2 $CD4^+$ T cells can enhance the expression of *Il17* and *Ifng* by 2D2 $CD4^+$ T cells (Fig 7E). Additionally, we found that P3 could activate DCs by stimulating the expression of CD80 and MHC II (Fig 7F).

Discussion

The gut microbiota has been implicated in the development of autoimmune diseases. Investigations of MS patients and the EAE mouse model have revealed that the gut microbiome is a crucial factor in disease progression and severity (4, 5). Alterations in gut bacterial composition, including reductions in butyrate-producing bacteria and increases in *Akkermansia* and *Clostridia* populations have been consistently observed in MS patients (5, 7). Moreover, transfer of microbiota from MS patients to animal models has been shown to increase disease incidence,

suggesting that alterations in the microbiome may actively contribute to the development of MS (46). Germ-free and antibiotic-treated mice have shown resistance to EAE, further supporting the necessity of the microbiome for disease induction (47, 48).

Despite significant advances in understanding the role of the gut microbiota in MS pathogenesis, the underlying mechanisms leading to disease development remain poorly understood. Continuous sampling of gut microbial antigens by innate immune cells enhances the probability of presenting specific antigens to antigen-specific T cells. The presentation of these antigens is influenced by polymorphisms in MHC genes, suggesting a potential role for host-commensal microorganisms cross-reactivity in the development and persistence of autoimmunity among genetically predisposed individuals. Molecular mimicry has been proposed as a possible mechanism by which microorganisms can induce autoimmune diseases (15). According to this hypothesis, T cells that respond to an epitope derived from an infectious agent may cross-react with a self-antigen that shares sequence or structural similarities with the original microbial peptide (49). Evidence supporting this hypothesis has been observed in numerous autoimmune diseases, such as antiphospholipid syndrome and Type 1 Diabetes (50, 51). Given the diverse range of microorganisms in the gut, peptides derived from gut flora could potentially trigger the development of MS. The activation of autoreactive T cells is a critical component of the early autoimmune response in individuals who ultimately develop MS. While multiple potential antigens exist, MOG is a major EAE antigen in H-2b mice and a possible autoantigen in MS (21). The binding pattern of the MOG-MHC II-TCR complex has been characterized, revealing that tyrosine (Y) in position 40 of the MOG_{35-55} peptide is the dominant MHC II-binding residue, occupying the p1 pocket. Meanwhile, arginine (R) 41, phenylalanine (F) 44, R46, and valine (V) 47 are the major amino acids involved in TCR recognition (21). Research suggests that differences in the amino acid at position 42 between human MOG and mouse MOG may be associated with inducing B cell-dependent EAE (52). Further studies have shown that human MOG fails to induce EAE in mice with B cell antigen-presenting function deficiency (53). These findings collectively underscore the pivotal role of B cells as antigen-presenting cells in developing EAE. However, our current study aims to elucidate how auto-antigen mimic peptides derived from gut commensals stimulate auto-reactive T cells rather than focusing on the specific cell type responsible for presenting these mimic peptides as antigens. Therefore, we excluded this amino acid from our screening motif. Research suggests that low-affinity hotspot mimicry, which involves a subset of crucial residues within the TCR-binding footprint, rather than high-affinity structural mimicry, maybe a more common contributor to the initiation of autoimmune diseases (14, 21). In our study, we focused on identifying MOG_{35-55} mimics based on the similarity of essential residues within the TCR-binding footprint, enabling a broader screening of potential

target peptides in the gut microbiome that could induce MS.

Various immune cells play crucial roles in the pathophysiology of MS and EAE. $CD4^+$ T cells are central in coordinating the adaptive immune response, releasing cytokines and chemokines that activate myelin-specific $CD4^+$ T cells and promote their infiltration into the brain (54). Both IFN-γ-producing Th1 and IL-17-producing Th17 cells can induce EAE by activating CNS macrophages and microglia, leading to local inflammation and tissue damage (55). Our use of the MHC II-peptide-TCR recognition pattern for screening mimic analogs is driven by the pivotal role of $CD4^+$ T cells in EAE pathogenesis. Besides $CD4^+$ T cells, $CD8^+$ T cells also contribute significantly to MS development, as shown by disease induction through the transfer of myelin antigen-specific $CD8^+$ T cells in EAE (56). B cells also participate in MS pathogenesis by presenting antigenic peptides to T cells (53), producing cytokines and contributing to the differentiation of lymphocyte subpopulations. Given the diverse functions of B cells, it is possible that gut microbiota mimics could also impact certain B cell-associated autoimmune diseases through the recognition by B cells. Additionally, recent research implicates neutrophils in MS pathogenesis, with their depletion before disease onset ameliorated symptoms (57). Neutrophils recruited to the brain by $CD4^+$ T cells can exacerbate parenchymal inflammation. Despite the contributions of various immune cells in MS, $CD4^+$ T cells remain central to its pathogenesis. Our study suggests that the exogenous antigens from the gut may activate autoreactive $CD4^+$ T cells through molecular mimicry.

By leveraging the expanding genome databases for human gut microbes, we identified 8 microbial peptides that exhibit significant analogy in their antigen-MHC II-TCR binding patterns with $MOG_{35\text{-}55}$ peptide. Our findings indicated that microbiome-derived P3 can activate $CD4^+$ T cells specific to $MOG_{35\text{-}55}$ peptide in mice. During the screening process, peptides like P2 and P4 exhibited only a single amino acid difference from the core sequence of P3, yet did not demonstrate encephalitogenic capacity like P3. This discrepancy may stem from the potential impact of individual amino acid variations on the spatial structure affecting the binding of peptides to MHC II and TCR (58). This observation suggests that in future studies, it may be necessary to evaluate the influence of single amino acid variances on the spatial structure affecting the binding of MHC II-peptide-TCR complex. Interestingly, our bioinformatic analysis revealed that P3 was derived from *A. muciniphila*, suggesting a potential impact of *A. muciniphila* on EAE development. Previous studies have explored the link between *A. muciniphila* and EAE or MS, such as the findings of Cekanaviciute *et al*., who observed that *A. muciniphila* promotes Th1 differentiation in human peripheral blood mononuclear cells (5). Moreover, previous studies have demonstrated that a peptide from *A. muciniphila* shares a similar sequence with an MS-associated self-antigen, guanosine diphosphate (GDP)–L-fucose synthase. This shared peptide sequence has the ability to stimulate the proliferation of $CD4^+$ cerebrospinal fluid-infiltrating T cells from

MS patients (16). In this study, we optimized the process of screening self-antigen mimics from gut microbiota by integrating the binding affinity to MHC II and TCR into the selection criteria, thereby enhancing the accuracy of identifying self-antigen analogs in the gut microbiome. Furthermore, our findings suggest that the enrichment of *A. muciniphila* in the gut microbiota of EAE mice and MS patients may have pathological implications as this bacterium has the capability of generating MOG_{35-55} analogs.

A. muciniphila, a next-generation probiotic, has shown positive effects on several diseases including obesity and diabetes (59). However, recent studies have revealed an enrichment of *A. muciniphila* in the gut microbiome of MS patients. Furthermore, transplantation of fecal samples from MS patients into the intestines of EAE mice leads to more severe EAE symptoms (5), indicating the need to assess the potential beneficial or harmful effects of *A. muciniphila* from multiple perspectives. Although multiple strains of *A. muciniphila* have been identified (60), it remains unclear whether the observed effects in different disease contexts are attributable to strain differences. The predominant use of metagenomics and 16S sequencing in numerous studies exploring the relationship between various diseases and *A. muciniphila* has impeded the identification of specific target strains, as these methods primarily facilitate gene annotation at the species level, presenting challenges in strain-level identification. Our study suggests that *A. muciniphila* may contribute to the development of EAE due to its capacity to generate MOG_{35-55}-resembling peptides. However, more evidence is needed to determine the target strain that generates MOG_{35-55} analogs. Future studies will also focus on elucidating the role of synergistic or antagonistic effect among different microbial populations in autoimmune diseases. This study highlights the necessity for further research on the correlation between gut microbiota and autoimmune diseases in the growing trend of widespread probiotic consumption.

In summary, our findings prove a mechanism of molecular mimicry in which a particular sequence within commensal gut microbe can imitate crucial residues in the MOG-MHC II-TCR binding footprint, consequently initiating or modifying the immune response associated with EAE development. While our study focused only on MOG_{35-55} mimics, other myelin antigens, such as MBP and proteolipid protein, may also serve as targets for autoreactive $CD4^+$ T cells (61). Given the enormous number of microbial peptides generated by the gut microbiota, it is possible that other microbial peptides may exist and can mimic these antigens and activate related autoantigen-reactive T cells. Meanwhile, it's important to note that the induction of autoimmune diseases through molecular mimicry is complicated and a single factor acting alone is unlikely to trigger the disease. Instead, accompanying host genetic susceptibility is considered to be linked with an abnormal immune response triggered by one or more microbial antigens or molecules. Nonetheless, this discovery may provide a therapeutic target and an

opportunity to impede the progression of MS.

Our data suggests the potential involvement of a MOG_{35-55}-mimic peptide derived from the gut microbiota as a molecular trigger of EAE pathogenesis. However, the limitations of this work must be acknowledged. First, while metagenomic approaches are valuable, they have inherent limitations in identifying specific bacteria strains. The prevalent focus on gene annotation at the species level in metagenomics and 16S sequencing restricts strain-level identification (62). Although marker-based computational methods provide strain-level sensitivity (63), they often operate under a single dominant strain per species, thereby overlooking the complex mixture of closely related strains within human-associated microbiota (64). Our methodology utilizing metagenomic data cannot identify the specific *A. muciniphila* strain capable of producing MOG_{35-55} analogs. These challenges underscore a limitation in our ability to identify the precise *A. muciniphila* strain of interest.

Collectively, we have investigated the role of molecular mimicry in the link between microbial flora and EAE development. We have identified MOG_{35-55} mimics derived from gut commensal cross-react with MOG_{35-55}-specific $CD4^+$ T cells and induce EAE in some mice. The combination immunization of this mimic and MOG_{35-55} significantly exacerbates the development of EAE in mice. Notably, antigen-presenting assays confirmed that DCs can process and present this gut commensal-derived peptide to MOG_{35-55}-specific $CD4^+$ T cells. Our findings offer direct evidence of how microbes can initiate the development of EAE, suggesting a potential microbiome-based therapeutic target for inhibiting the progression of MS.

Contributors: Conceptualization: GY, YXL; Methodology: XM, JZ, QLJ; Investigation: XM, JZ; Visualization: XM, JZ; Supervision: GY, YXL; Writing: XM, JZ, YXL, GY. XM and JZ have directly accessed and verified the underlying data reported in the manuscript. GY and YXL are responsible for the decision to submit the manuscript.

Data Sharing Statement: All study data are included in the article and/or Supplementary files.

Declaration of interests: The authors declare no competing interests.

Acknowledgments: This work is supported by the National Natural Science Foundation of China (82371350). The funding source has no role in the writing of the manuscript or the decision to submit it for publication.

Reference

1. Sospedra M, Martin R. Immunology of multiple sclerosis. Annu Rev Immunol. 2005;23:683-747.
2. Walton C, King R, Rechtman L, Kaye W, Leray E, Marrie RA, et al. Rising prevalence of multiple sclerosis worldwide: Insights from the Atlas of MS. Multiple Sclerosis Journal. 2020;26(14):1816-21.
3. Alroughani R, Boyko A. Pediatric multiple sclerosis: a review. BMC neurology. 2018;18:1-8.
4. Lee YK, Menezes JS, Umesaki Y, Mazmanian SK. Proinflammatory T-cell responses to gut microbiota promote experimental autoimmune encephalomyelitis. Proceedings of the National Academy of Sciences. 2011;108(supplement_1):4615-22.
5. Cekanaviciute E, Yoo BB, Runia TF, Debelius JW, Singh S, Nelson CA, et al. Gut bacteria from multiple sclerosis patients modulate human T cells and exacerbate symptoms in mouse models. Proceedings of the National Academy of Sciences. 2017;114(40):10713-8.
6. Chen J, Chia N, Kalari KR, Yao JZ, Novotna M, Paz Soldan MM, et al. Multiple sclerosis patients have a distinct gut microbiota compared to healthy controls. Scientific reports. 2016;6(1):28484.
7. Jangi S, Gandhi R, Cox LM, Li N, Von Glehn F, Yan R, et al. Alterations of the human gut microbiome in multiple sclerosis. Nature communications. 2016;7(1):12015.
8. Johanson DM, Goertz JE, Marin IA, Costello J, Overall CC, Gaultier A. Experimental autoimmune encephalomyelitis is associated with changes of the microbiota composition in the gastrointestinal tract. Scientific reports. 2020;10(1):15183.
9. Rojas M, Restrepo-Jiménez P, Monsalve DM, Pacheco Y, Acosta-Ampudia Y, Ramírez-Santana C, et al. Molecular mimicry and autoimmunity. Journal of autoimmunity. 2018;95:100-23.
10. Greiling TM, Dehner C, Chen X, Hughes K, Iñiguez AJ, Boccitto M, et al. Commensal orthologs of the human autoantigen Ro60 as triggers of autoimmunity in lupus. Science Translational Medicine. 2018;10(434):eaan2306.
11. Naghavian R, Faigle W, Oldrati P, Wang J, Toussaint NC, Qiu Y, et al. Microbial peptides activate tumour-infiltrating lymphocytes in glioblastoma. Nature. 2023:1-11.
12. Kalaora S, Nagler A, Nejman D, Alon M, Barbolin C, Barnea E, et al. Identification of bacteria-derived HLA-bound peptides in melanoma. Nature. 2021;592(7852):138-43.
13. Gil-Cruz C, Perez-Shibayama C, De Martin A, Ronchi F, Van Der Borght K, Niederer R, et al. Microbiota-derived peptide mimics drive lethal inflammatory cardiomyopathy. Science. 2019;366(6467):881-6.
14. Harkiolaki M, Holmes SL, Svendsen P, Gregersen JW, Jensen LT, McMahon R, et al. T cell-mediated autoimmune disease due to low-affinity crossreactivity to common microbial peptides. Immunity. 2009;30(3):348-57.
15. Wucherpfennig KW, Strominger JL. Molecular mimicry in T cell-mediated autoimmunity: viral peptides activate human T cell clones specific for myelin basic protein. Cell. 1995;80(5):695-705.
16. Planas R, Santos R, Tomas-Ojer P, Cruciani C, Lutterotti A, Faigle W, et al. GDP-l-fucose synthase is a CD4+ T cell–specific autoantigen in DRB3* 02: 02 patients with multiple sclerosis. Science translational medicine. 2018;10(462):eaat4301.
17. Fujinami RS, Oldstone MB. Amino acid homology between the encephalitogenic site of myelin basic protein and virus: mechanism for autoimmunity. Science. 1985;230(4729):1043-5.
18. Lerch M, Bauer A, Reindl M. The Potential pathogenicity of myelin oligodendrocyte glycoprotein antibodies in the optic pathway. Journal of Neuro-Ophthalmology. 2023;43(1):5.
19. Marignier R, Hacohen Y, Cobo-Calvo A, Pröbstel A-K, Aktas O, Alexopoulos H, et al. Myelin-oligodendrocyte glycoprotein antibody-associated disease. The Lancet Neurology. 2021;20(9):762-72.
20. Reindl M, Waters P. Myelin oligodendrocyte glycoprotein antibodies in neurological disease. Nature Reviews Neurology. 2019;15(2):89-102.
21. Petersen TR, Bettelli E, Sidney J, Sette A, Kuchroo V, Backstrom BT. Characterization of MHC- and TCR-binding residues of the myelin oligodendrocyte glycoprotein 38-51

peptide. Eur J Immunol. 2004;34(1):165-73.
22. Almeida A, Nayfach S, Boland M, Strozzi F, Beracochea M, Shi ZJ, et al. A unified catalog of 204,938 reference genomes from the human gut microbiome. Nat Biotechnol. 2021;39(1):105-14.
23. Pasolli E, Asnicar F, Manara S, Zolfo M, Karcher N, Armanini F, et al. Extensive Unexplored Human Microbiome Diversity Revealed by Over 150,000 Genomes from Metagenomes Spanning Age, Geography, and Lifestyle. Cell. 2019;176(3):649-62 e20.
24. Chaumeil PA, Mussig AJ, Hugenholtz P, Parks DH. GTDB-Tk v2: memory friendly classification with the genome taxonomy database. Bioinformatics. 2022;38(23):5315-6.
25. Kishikawa T, Ogawa K, Motooka D, Hosokawa A, Kinoshita M, Suzuki K, et al. A Metagenome-Wide Association Study of Gut Microbiome in Patients With Multiple Sclerosis Revealed Novel Disease Pathology. Front Cell Infect Microbiol. 2020;10:585973.
26. Li D, Liu CM, Luo R, Sadakane K, Lam TW. MEGAHIT: an ultra-fast single-node solution for large and complex metagenomics assembly via succinct de Bruijn graph. Bioinformatics. 2015;31(10):1674-6.
27. von Meijenfeldt FAB, Arkhipova K, Cambuy DD, Coutinho FH, Dutilh BE. Robust taxonomic classification of uncharted microbial sequences and bins with CAT and BAT. Genome Biol. 2019;20(1):217.
28. Parks DH, Chuvochina M, Rinke C, Mussig AJ, Chaumeil PA, Hugenholtz P. GTDB: an ongoing census of bacterial and archaeal diversity through a phylogenetically consistent, rank normalized and complete genome-based taxonomy. Nucleic Acids Res. 2022;50(D1):D785-D94.
29. Santos-Aberturas J, Chandra G, Frattaruolo L, Lacret R, Pham TH, Vior NM, et al. Uncovering the unexplored diversity of thioamidated ribosomal peptides in Actinobacteria using the RiPPER genome mining tool. Nucleic Acids Res. 2019;47(9):4624-37.
30. Motmaen A, Dauparas J, Baek M, Abedi MH, Baker D, Bradley P. Peptide-binding specificity prediction using fine-tuned protein structure prediction networks. Proc Natl Acad Sci U S A. 2023;120(9):e2216697120.
31. Mikhaylov V, Levine AJ. Accurate modeling of peptideMHC structures with AlphaFold. 2023.
32. Bradley P. Structure-based prediction of T cell receptor:peptide-MHC interactions. Elife. 2023;12.
33. Marzella DF, Parizi FM, van Tilborg D, Renaud N, Sybrandi D, Buzatu R, et al. PANDORA: A Fast, Anchor-Restrained Modelling Protocol for Peptide: MHC Complexes. Front Immunol. 2022;13:878762.
34. Reynisson B, Barra C, Kaabinejadian S, Hildebrand WH, Peters B, Nielsen M. Improved Prediction of MHC II Antigen Presentation through Integration and Motif Deconvolution of Mass Spectrometry MHC Eluted Ligand Data. J Proteome Res. 2020;19(6):2304-15.
35. Motmaen A, Dauparas J, Baek M, Abedi MH, Baker D, Bradley P. Peptide-binding specificity prediction using fine-tuned protein structure prediction networks. Proceedings of the National Academy of Sciences. 2023;120(9):e2216697120.
36. La Gruta NL, Gras S, Daley SR, Thomas PG, Rossjohn J. Understanding the drivers of MHC restriction of T cell receptors. Nat Rev Immunol. 2018;18(7):467-78.
37. Steimle A, Neumann M, Grant ET, Willieme S, De Sciscio A, Parrish A, et al. Gut microbial factors predict disease severity in a mouse model of multiple sclerosis. Nature Microbiology. 2024;9(9):2244-61.
38. Yang G, Postoak JL, Song W, Martinez J, Zhang J, Wu L, et al. Dendritic cell PIK3C3/VPS34 controls the pathogenicity of CNS autoimmunity independently of LC3-associated phagocytosis. Autophagy. 2022;18(1):161-70.
39. Quan M-Y, Song X-J, Liu H-J, Deng X-H, Hou H-Q, Chen L-P, et al. Amlexanox attenuates experimental autoimmune encephalomyelitis by inhibiting dendritic cell maturation and reprogramming effector and regulatory T cell responses. Journal of neuroinflammation. 2019;16:1-17.
40. Almeida A, Nayfach S, Boland M, Strozzi F, Beracochea M, Shi ZJ, et al. A unified catalog of 204,938 reference genomes from the human gut microbiome. Nature biotechnology. 2021;39(1):105-14.

41. Kishikawa T, Ogawa K, Motooka D, Hosokawa A, Kinoshita M, Suzuki K, et al. A metagenome-wide association study of gut microbiome in patients with multiple sclerosis revealed novel disease pathology. Frontiers in cellular and infection microbiology. 2020;10:585973.
42. Zhou X, Baumann R, Gao X, Mendoza M, Singh S, Sand IK, et al. Gut microbiome of multiple sclerosis patients and paired household healthy controls reveal associations with disease risk and course. Cell. 2022;185(19):3467-86. e16.
43. Ishina IA, Zakharova MY, Kurbatskaia IN, Mamedov AE, Belogurov AA, Jr., Gabibov AG. MHC Class II Presentation in Autoimmunity. Cells. 2023;12(2).
44. Pishesha N, Harmand TJ, Ploegh HL. A guide to antigen processing and presentation. Nat Rev Immunol. 2022;22(12):751-64.
45. Lourbopoulos A, Deraos G, Matsoukas MT, Touloumi O, Giannakopoulou A, Kalbacher H, et al. Cyclic MOG(35)(-)(55) ameliorates clinical and neuropathological features of experimental autoimmune encephalomyelitis. Bioorg Med Chem. 2017;25(15):4163-74.
46. Berer K, Gerdes LA, Cekanaviciute E, Jia X, Xiao L, Xia Z, et al. Gut microbiota from multiple sclerosis patients enables spontaneous autoimmune encephalomyelitis in mice. Proceedings of the National Academy of Sciences. 2017;114(40):10719-24.
47. Berer K, Mues M, Koutrolos M, Rasbi ZA, Boziki M, Johner C, et al. Commensal microbiota and myelin autoantigen cooperate to trigger autoimmune demyelination. Nature. 2011;479(7374):538-41.
48. Ochoa-Repáraz J, Mielcarz DW, Ditrio LE, Burroughs AR, Foureau DM, Haque-Begum S, et al. Role of gut commensal microflora in the development of experimental autoimmune encephalomyelitis. The Journal of Immunology. 2009;183(10):6041-50.
49. Ochoa-Repáraz J, Kirby TO, Kasper LH. The gut microbiome and multiple sclerosis. Cold Spring Harbor perspectives in medicine. 2018;8(6).
50. Ruff WE, Dehner C, Kim WJ, Pagovich O, Aguiar CL, Andrew TY, et al. Pathogenic autoreactive T and B cells cross-react with mimotopes expressed by a common human gut commensal to trigger autoimmunity. Cell host & microbe. 2019;26(1):100-13. e8.
51. Girdhar K, Huang Q, Chow I-T, Vatanen T, Brady C, Raisingani A, et al. A gut microbial peptide and molecular mimicry in the pathogenesis of type 1 diabetes. Proceedings of the National Academy of Sciences. 2022;119(31):e2120028119.
52. Oliver AR, Lyon GM, Ruddle NH. Rat and human myelin oligodendrocyte glycoproteins induce experimental autoimmune encephalomyelitis by different mechanisms in C57BL/6 mice. The Journal of Immunology. 2003;171(1):462-8.
53. Molnarfi N, Schulze-Topphoff U, Weber MS, Patarroyo JC, Prod'homme T, Varrin-Doyer M, et al. MHC class II–dependent B cell APC function is required for induction of CNS autoimmunity independent of myelin-specific antibodies. Journal of Experimental Medicine. 2013;210(13):2921-37.
54. Wang J, Jelcic I, Mühlenbruch L, Haunerdinger V, Toussaint NC, Zhao Y, et al. HLA-DR15 molecules jointly shape an autoreactive T cell repertoire in multiple sclerosis. Cell. 2020;183(5):1264-81. e20.
55. Næss LM, Oftung F, Aase A, Michaelsen TE, Pollard AJ. T-cell responses against meningococcal antigens. Meningococcal Vaccines: Methods and Protocols. 2001:339-48.
56. Huseby ES, Liggitt D, Brabb T, Schnabel B, Öhlén C, Goverman J. A pathogenic role for myelin-specific CD8+ T cells in a model for multiple sclerosis. The Journal of experimental medicine. 2001;194(5):669-76.
57. McColl SR, Staykova MA, Wozniak A, Fordham S, Bruce J, Willenborg DO. Treatment with anti-granulocyte antibodies inhibits the effector phase of experimental autoimmune encephalomyelitis. The Journal of Immunology. 1998;161(11):6421-6.
58. Huseby ES, Crawford F, White J, Marrack P, Kappler JW. Interface-disrupting amino acids establish specificity between T cell receptors and complexes of major histocompatibility complex and peptide. Nature immunology. 2006;7(11):1191-9.
59. Cani PD, Depommier C, Derrien M, Everard A, de Vos WM. Akkermansia muciniphila: paradigm for next-generation beneficial microorganisms. Nature Reviews Gastroenterology & Hepatology. 2022;19(10):625-37.
60. Guo X, Zhang J, Wu F, Zhang M, Yi M, Peng Y. Different subtype strains of Akkermansia muciniphila abundantly colonize in southern China. Journal of applied

microbiology. 2016;120(2):452-9.
61. Greer JM. Autoimmune T-cell reactivity to myelin proteolipids and glycolipids in multiple sclerosis. Multiple sclerosis international. 2013;2013.
62. Albanese D, Donati C. Strain profiling and epidemiology of bacterial species from metagenomic sequencing. Nature communications. 2017;8(1):2260.
63. Scholz M, Ward DV, Pasolli E, Tolio T, Zolfo M, Asnicar F, et al. Strain-level microbial epidemiology and population genomics from shotgun metagenomics. Nature methods. 2016;13(5):435-8.
64. Oh J, Byrd AL, Park M, Kong HH, Segre JA. Temporal stability of the human skin microbiome. Cell. 2016;165(4):854-66.

Figure legends

Figure 1. Overview of MOG_{35-55} analogs identified in the human microbiome.

(A) The workflow of human microbiome-derived peptides discovery. (B) The proportion of MOG_{35-55} analogs with well-defined binding motifs. (C) Chord diagram showing the taxonomy distribution of prioritized analogs. The values in brackets show the total number of analogs with corresponding binding motifs. per genome in each phylum. The counts of analogs in each phylum were normalized by the genome counts. The scale was the proportion of analogs in each motif (upper) or in each phylum. Of note, the genomes less than 10 counts from *Firmicutes_I*, *Firmicutes_B*, *Bacillota_B*, *Cyanobacteria*, *Desulfobacterota_I*, *Fusobacteriota*, *Pseudomonadota*, *Euryarchaeota*, *Halobacterota*, *Patescibacteria*, and 19 unclassified contigs were merged into Others.

Figure 2. The confidence of $hMOG_{35-55}$ binding core peptide-MHC II and peptide-MHC II-TCR complexes predicted TCRDock.

The scatter plots show the peptides' per-residue confidence score (pLDDT) value of a peptide versus an averaged inter-chain PAE of peptide-MHC-II complexes (A) and peptide-MHC II-TCR complexes (B) for binding core peptide candidates chopped from human MOG_{35-55}. The predicted MHC II binding peptides (pLDDT ≥ 90, inter-PAE ≤ 4.34) are highlighted in red. The sequence of binding core peptide candidates is listed on the right side of panel A. The modeling of a peptide with pLDDT≥ 70 is considered as confident. (C) Predicted structure of peptide-MHC II-TCR complex with binding core peptide derived from MOG_{35-55}. TCR alleles same from complex template 3rdt (PDB ID). Surface representation is displayed in lighter shades. (D) Close-up view of peptide-TCR interactions (upper) and peptide-MHC II (bottom), colored amino acid residues represent the dominant MHC II-binding residue (green) and major TCR recognition residue (red). Peptide residues and TCR alpha CDR1 and CDR3 (orange) and TCR beta CDR3 (hot pink) residues were shown in sticks, and residues from MHC II interacting with peptide were shown in slate blue. Hydrogen bonds are highlighted in black dashed lines.

Figure 3. Polymorphism in 9-mer binding core peptides of the predicted peptide-MHC II complex.

(A) The stacked bar plot shows the number of nonredundant ligands with 11 amino acids residues truncated from analogs, colored with different motifs. (B) The scatter plot shows the pLDDT value of a binding core peptide (corresponding to local structural accuracy) versus an averaged MHC II-peptide complex's inter-chain PAE score (corresponding to the peptide-MHC II interactions). The predicted binder is highlighted in red. (C) The frequencies of amino acid residues (rows) at specific positions (columns) among the predicted MHC II binding peptides. The loc_1 ~ loc_9 represent the binding core region among the binder, and loc_0 and loc_10

represent the flanking region of binders. (D) Representative sequence logos illustrating peptide residue preference of MHC II. Each logo is labeled with the starting amino acid residue of binding core peptides, and the number of binding core peptides used to generate the logos is paired to the corresponding cells in panel [B]. The logos are colored by the chemical polarity of the amino acid residue. In panels C and D, sequence/residue numbers are 0-indexed: they start at 0 and end with N-1, where N is the length of the sequence.

Figure 4. Microbiome-derived peptide can stimulate MOG_{35-55}-specific T cells from EAE mice.

(A) The origin and sequence of microbial peptides tested in this study. The amino acids highlighted in green are the dominant MHC II-binding residue, while major TCR contact residues are colored in red. The amino acids colored in blue represent different residue between human MOG_{35-55} and mouse MOG_{35-55}. The asterisk highlights that P5 is a peptide predicted in both *Alistipes putredinis* and *A. muciniphila*. (B-D) MOG_{35-55}–specific $CD4^+$ T cells collected from the spleen of EAE mice (n = 3) were treated with each of the 8 selected microbial peptides. PBS and MOG_{35-55} were served as negative control and positive control; Scrambled peptide was set as a peptide control. Flow cytometry was used to determine IFN-γ and IL-17 production. Representative FACS plots (gated on $CD3^+CD4^+$ cells) for the population of IFN-γ- or IL-17-secreted $CD4^+$ T cells that were stimulated with mimic peptides or MOG_{35-55} (20 µg/ml final concentration). Only data from P3, which induced the highest cytokine-producing cell population was shown (B), along with the frequency (C) and cell count (D) of each population among $CD4^+$ T cells. (E, F) Mice (n = 4) immunized with MOG_{35-55} were sacrificed at 17 dpi. Immune cells from the spinal cord were collected and then stimulated with either MOG_{35-55} (positive control), P3, scrambled peptide, or PBS in a concentration of 20 µg/ml. Representative FACS plots demonstrate the population of activated $CD4^+$ T cells (E), along with the frequency (F) of IL-17^+ and IFN-γ^+ population among $CD4^+$ T cells. Results shown are representative of three independent experiments. Data shown are the average ± SEM. *$p < 0.05$, **$p < 0.01$.

Figure 5. P3 shows encephalitogenic capacity *in vivo*.

(A) Experimental design of EAE induction. (B) Mean EAE clinical scores and (C) Kaplan-Meier curve of disease-free survival from mice immunized with either P3, MOG_{35-55}, or CFA control. Mice (n = 12) were immunized on day 0 and assessed daily by standard disease scoring for 26 consecutive days. Data shown are pooled from two independent experiments. (D) Experimental outline for adoptive transfer EAE. (E) Mean EAE clinical scores and (F) Kaplan-Meier curve of disease-free survival from mice received either splenocytes stimulated P3 (n = 7) or MOG_{35-55} (n = 3). Data shown are the average ± SEM.

Figure 6. P3 in combination with MOG_{35-55} exacerbates EAE development in mice.

(A) The illustration for the experimental design. (B) Mean EAE clinical scores from each group of mice (n = 8). The data shown are representative of two independent experiments. (C) Splenocytes (n = 5) from either P3 + MOG_{35-55} immunized mice or scrambled peptide + MOG_{35-55} immunized mice were stimulated with MOG_{35-55} in a concentration of 20 μg/ml (PBS as a negative stimulation). Representative FACS plots (gated on $CD3^+$ and $CD4^+$ cells) demonstrate the population of activated $CD4^+$ T cells, along with the frequency of IL-17^+ and INF-γ^+ population among $CD4^+$ T cells. (D) Spinal cord samples were collected at 17 dpi and the leukocyte population within the CNS was assessed by flow cytometry. The cell count of leukocytes was significantly higher in MOG_{35-55} + P3 group than MOG_{35-55} + scrambled peptide group (n = 8). (E, F) Spinal cord tissue sections were obtained at 17 dpi and stained with H&E (E) or LFB (F). The inflammatory level (H&E scores) and demyelination level (LFB scores) were quantified (n=4-5). Data shown are the average ± SEM. $^*p < 0.05$, $^{***}p < 0.001$.

Figure 7. P3 stimulates 2D2 $CD4^+$ T cell proliferation through DCs presentation *in vitro*.

(A) Predicted structure of peptide-MHC II-TCR complex with binding core peptide from P3. TCR alleles same from complex template 3c60 (PDB ID). Surface representation is displayed in lighter shades. (B) Close-up view of peptide-TCR interactions (upper) and peptide-MHC II (bottom) in panel D, colored amino acid residues represent the dominant MHC II-binding residue (green) and major TCR recognition residue (red). Peptide residues and TCR alpha CDR3 (orange) and TCR beta CDR3 (hot pink) residues were shown in sticks, and residues from MHC II interacting with peptide were shown in slate blue. Hydrogen bonds are highlighted in black dashed lines. (C, D) The histogram FACS plots (C) and quantification (D) of CFSE labeled 2D2 $CD4^+$ T cells proliferation (n = 3), as well as the frequency of $CD69^+$ cells within the $CD4^+$ T cells population, following co-culture with DCs pulsed with PBS, P3, or MOG_{35-55}. Dash line in histogram represents the proliferation level of PBS control. (E) The relative mRNA expression of *Il17a* and *Ifng* genes was determined by RT-qPCR. The mean expression levels are shown (n = 3). (F) DCs were isolated from C57BL/6J mice (n = 5) and stimulated with either MOG_{35-55}, P3, or scrambled peptide in a concentration of 20 μg/ml for 24 h and 48 h. The activation of DCs was assessed by measuring MFI of CD80, CD86, and MHC II. Results are representative of two independent experiments. Data shown are the average ± SEM. $^*p < 0.05$, $^{**}p < 0.01$, $^{***}p < 0.001$.

Figure 1

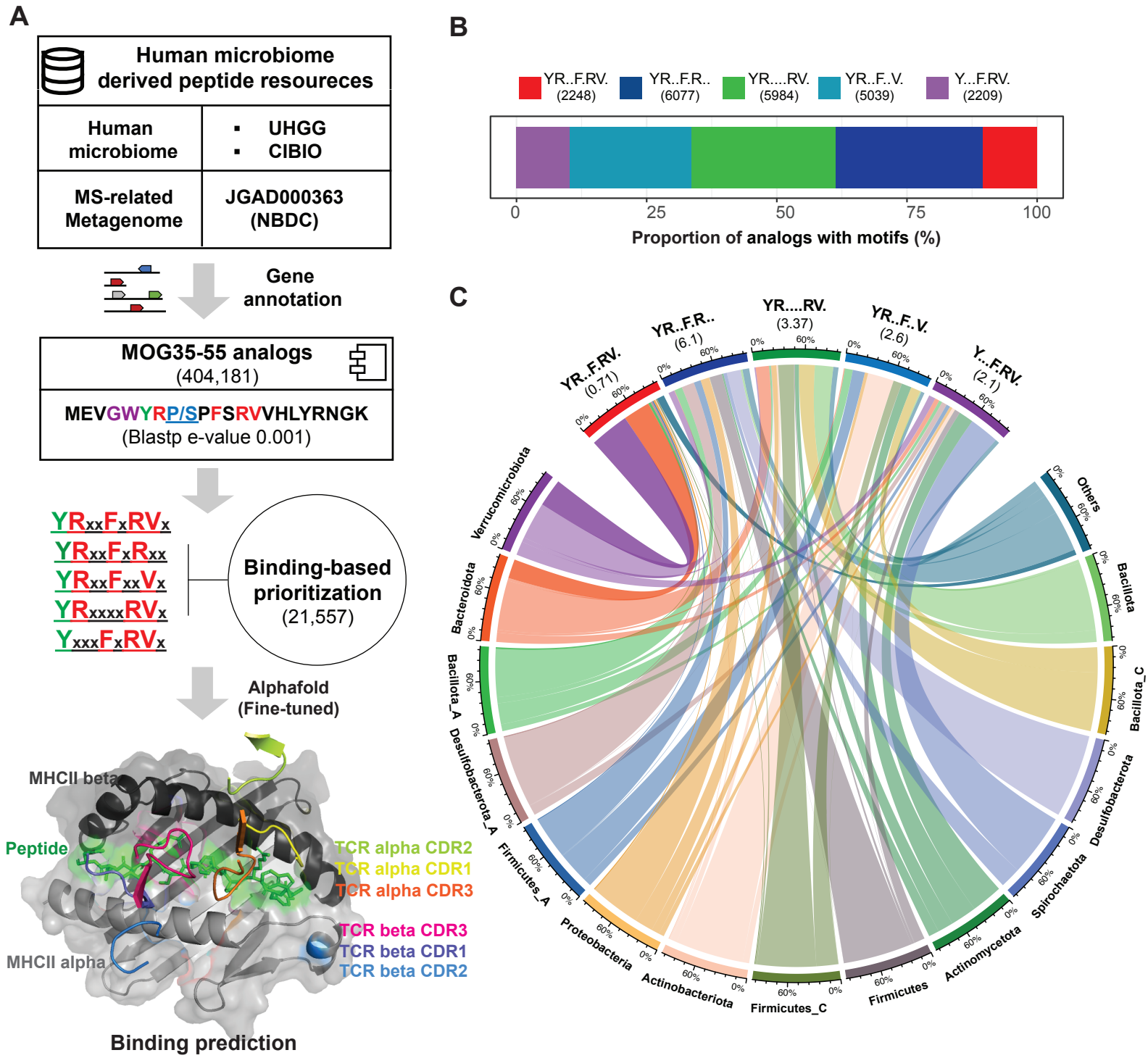
A
Human microbiome derived peptide resoureces
Human microbiome
UHGG
CIBIO
MS-related Metagenome
JGAD000363 (NBDC)
Gene annotation
MOG35-55 analogs (404,181)
MEVGWYRP/SPFSRVVHLYRNGK
(Blastp e-value 0.001)
YRxxFxRVx
YRxxFxRxx
YRxxFxxVx
YRxxxxRVx
YxxxFxRVx
Binding-based prioritization (21,557)
Alphafold (Fine-tuned)
MHCII beta
Peptide
MHCII alpha
TCR alpha CDR2
TCR alpha CDR1
TCR alpha CDR3
TCR beta CDR3
TCR beta CDR1
TCR beta CDR2
Binding prediction
B
YR..F.RV. (2248)
YR..F.R.. (6077)
YR....RV. (5984)
YR..F..V. (5039)
Y...F.RV. (2209)
0
25
50
75
100
Proportion of analogs with motifs (%)
C
YR..F.RV. (0.71)
YR..F.R.. (6.1)
YR....RV. (3.37)
YR..F..V. (2.6)
Y...F.RV. (2.1)
Verrucomicrobiota
Bacteroidota
Bacillota_A
Desulfobacterota_A
Firmicutes_A
Proteobacteria
Actinobacteriota
Firmicutes_C
Firmicutes
Actinomycetota
Spirochaetota
Desulfobacterota
Bacillota_C
Bacillota
Others

Figure 2

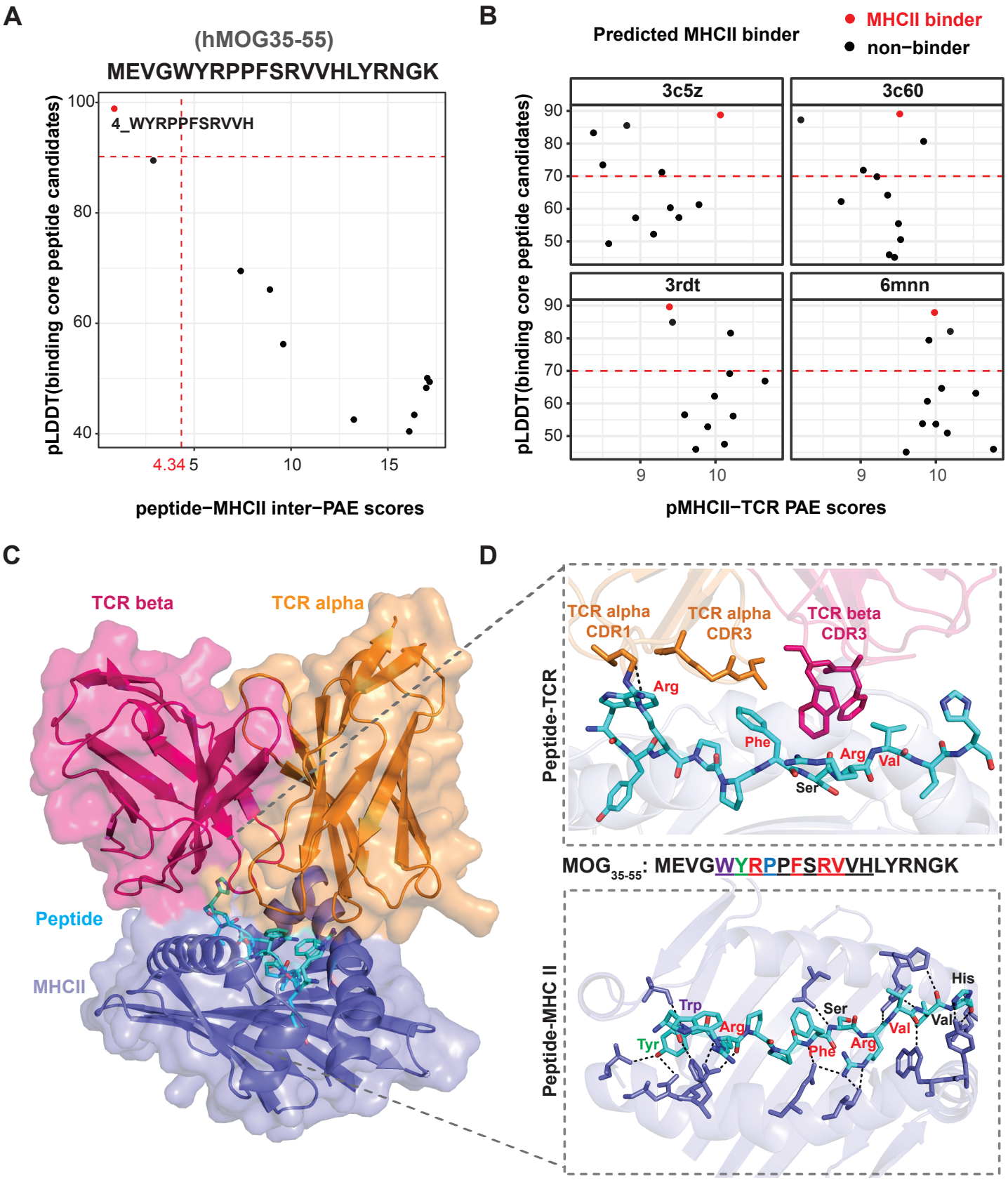
A
(hMOG35-55)
MEVGWYRPPFSRVVHLYRNGK
4_WYRPPFSRVVH
pLDDT(binding core peptide candidates)
peptide−MHCII inter−PAE scores
4.34
B
Predicted MHCII binder
MHCII binder
non−binder
3c5z
3c60
3rdt
6mnn
pLDDT(binding core peptide candidates)
pMHCII−TCR PAE scores
C
TCR beta
TCR alpha
Peptide
MHCII
D
TCR alpha CDR1
TCR alpha CDR3
TCR beta CDR3
Peptide-TCR
Arg
Phe
Arg
Val
Ser
MOG35-55: MEVGWYRPPFSRVVHLYRNGK
Peptide-MHC II
Trp
Tyr
Arg
Ser
Phe
Arg
Val
His
Val

Figure 3

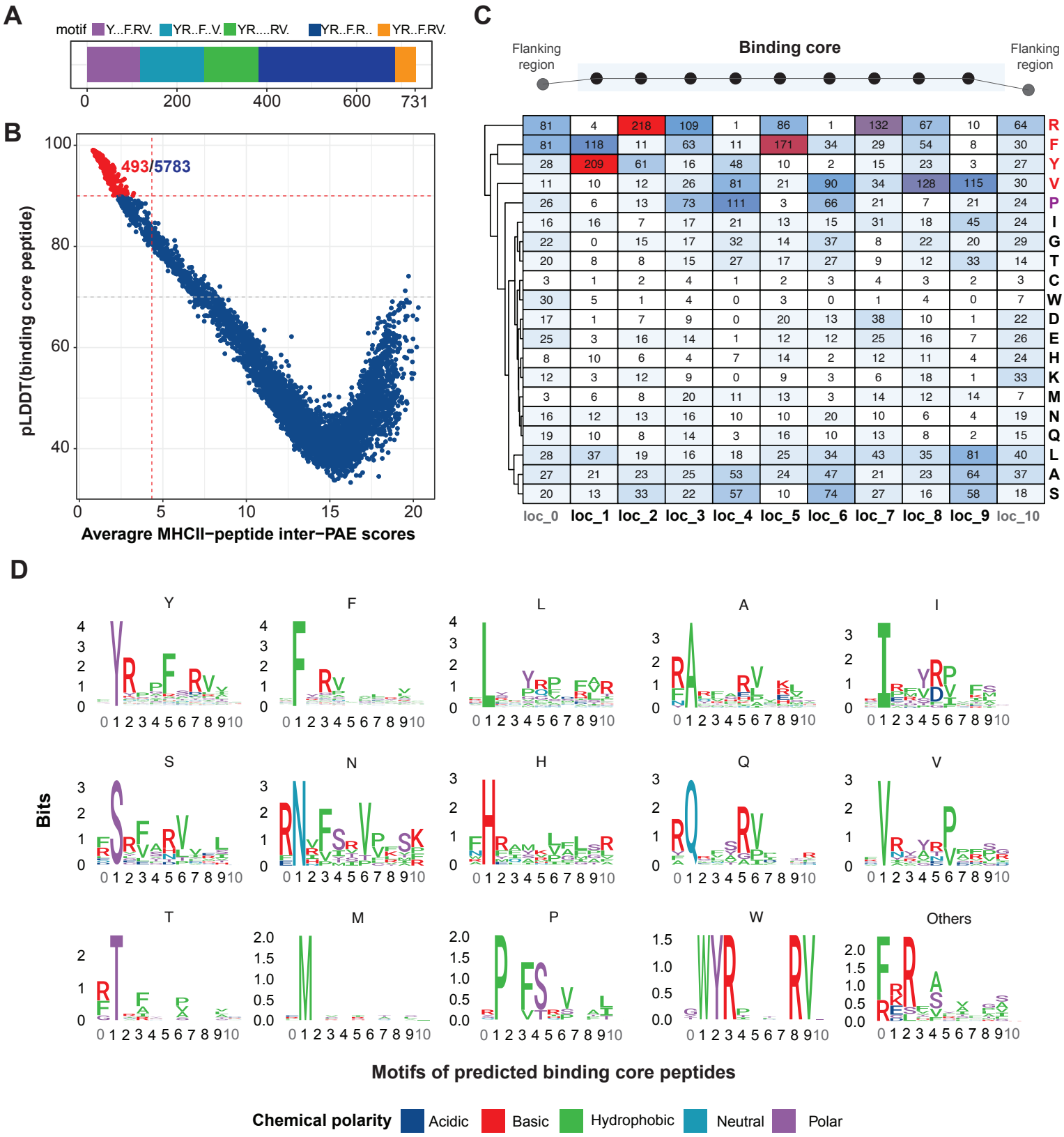
A
motif Y...F.RV. YR..F..V. YR....RV. YR..F.R.. YR..F.RV.
0 200 400 600 731
B
493/5783
pLDDT(binding core peptide)
Averagre MHCII−peptide inter−PAE scores
C
Flanking region
Binding core
Flanking region
R F Y V P I G T C W D E H K M N Q L A S
loc_0 loc_1 loc_2 loc_3 loc_4 loc_5 loc_6 loc_7 loc_8 loc_9 loc_10
D
Y F L A I S N H Q V T M P W Others
Bits
Motifs of predicted binding core peptides
Chemical polarity Acidic Basic Hydrophobic Neutral Polar

Figure 4

A

No	Taxonomy	Sequence
	Homo sapiens MOG$_{35-55}$	MEVGWYRPPFSRVVHLYRNGK
	Mus musculus MOG$_{35-55}$	MEVGWYRSPFSRVVHLYRNGK
P1	***Bacteroides*** MBL fold metallo-hydrolase	PIIYFYRSAFDRVMDGVKNSK
P2	***Alistipes sp902388705***	MDVNTYRPVFLRVPMDMILK
P3	***Akkermansia muciniphila***	TTLSFYRPPFLRVRRPFYIIF
P4	***Acutalibacteraceae***_UMGS1623 sp934647945	TFVQDYRYPFLRVISLLALAA
P5	***Alistipes putredinis, Akkermansia muciniphila***	AIDWFYRRPFSRVISETVFRY*
P6	***Bacteroides caccae***	LLLLWYRKIFVRVVWLGRTRH
P7	***Angelakisella***	EELEQYRPLFGRVIIRIRTPS
P8	***Pararuminococcus gallinarum***	KLKIKYREGFFRVVHAIRDFF

B

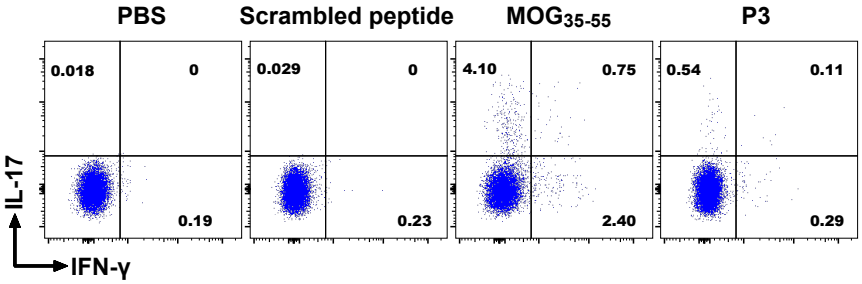

C

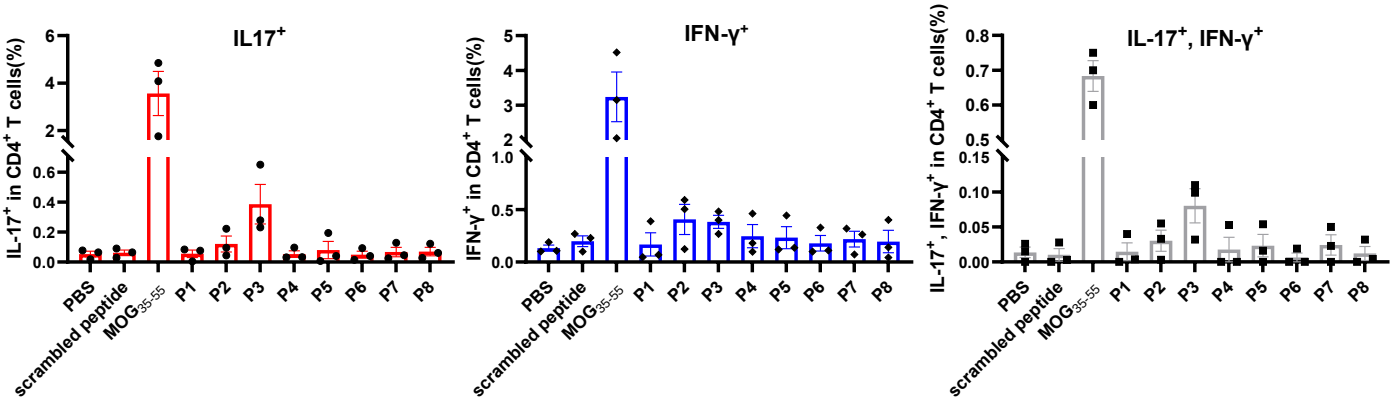

D

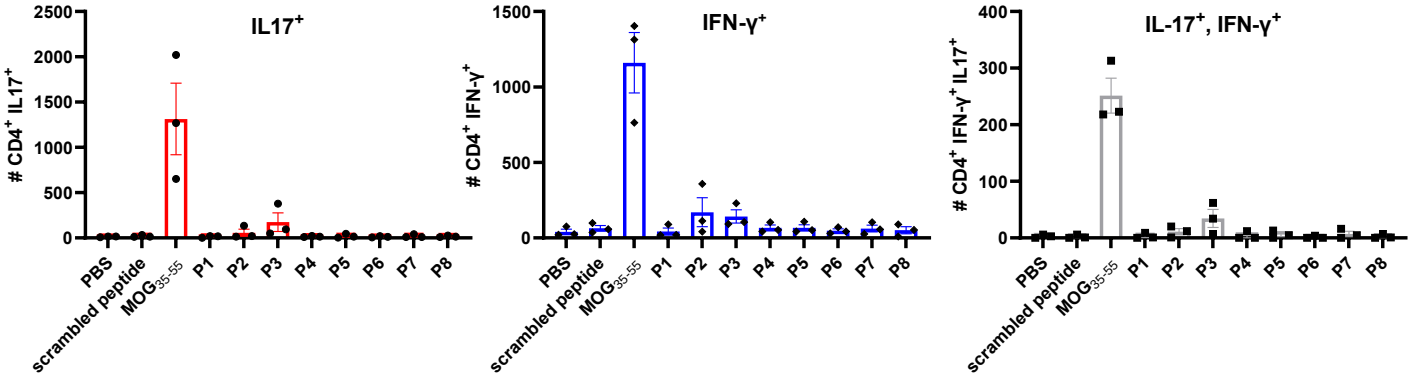

E

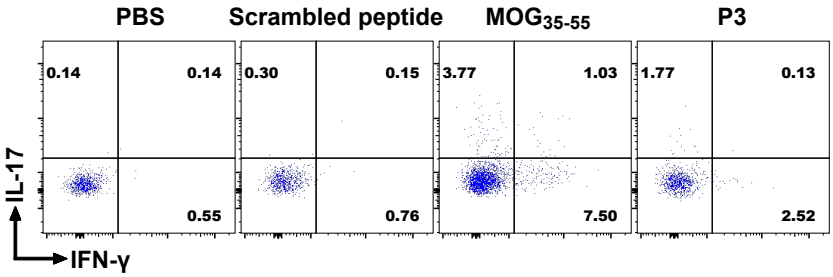

F

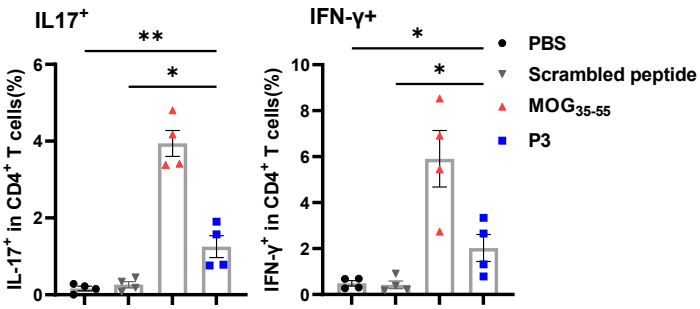

Figure 5

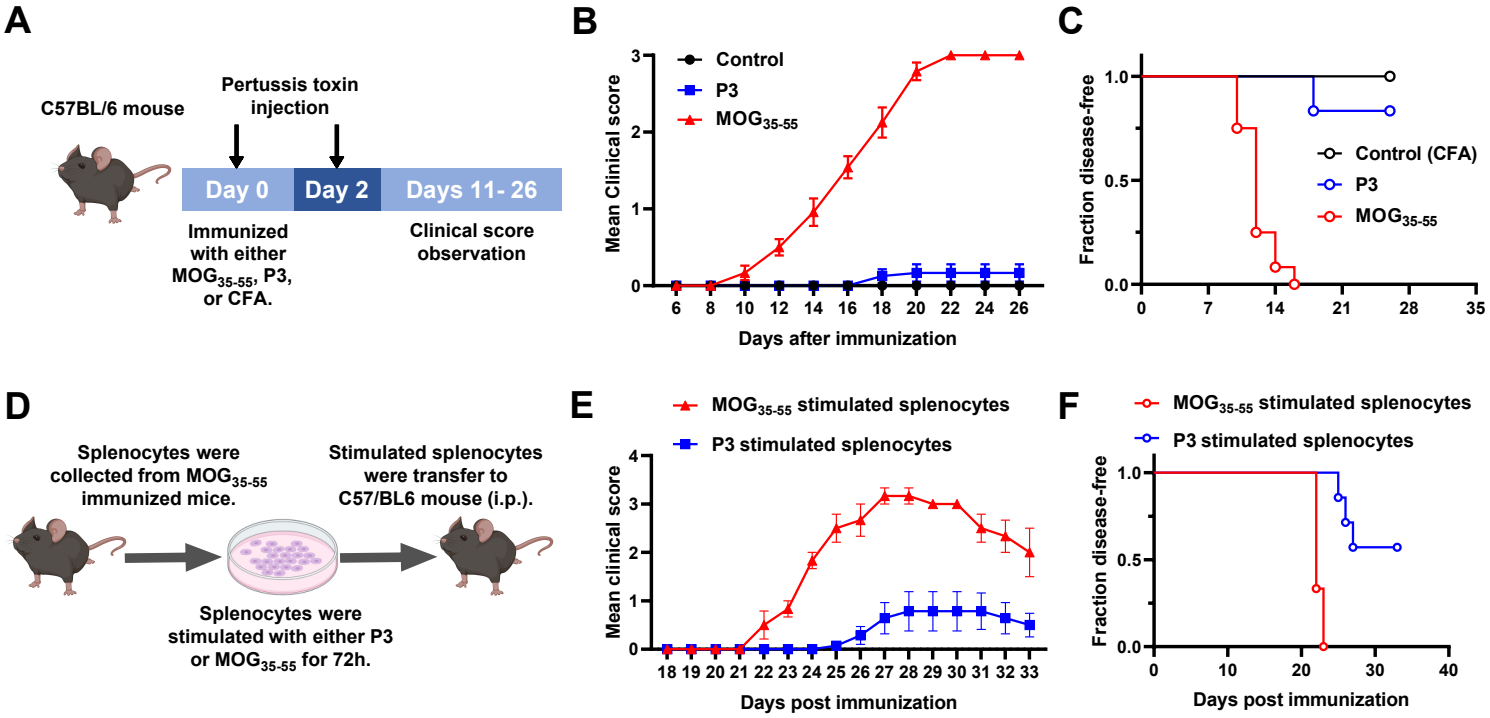
A
C57BL/6 mouse
Pertussis toxin injection
Day 0
Day 2
Days 11- 26
Immunized with either MOG35-55, P3, or CFA.
Clinical score observation
B
Control
P3
MOG35-55
Mean Clinical score
Days after immunization
C
Control (CFA)
P3
MOG35-55
Fraction disease-free
D
Splenocytes were collected from MOG35-55 immunized mice.
Stimulated splenocytes were transfer to C57/BL6 mouse (i.p.).
Splenocytes were stimulated with either P3 or MOG35-55 for 72h.
E
MOG35-55 stimulated splenocytes
P3 stimulated splenocytes
Mean clinical score
Days post immunization
F
MOG35-55 stimulated splenocytes
P3 stimulated splenocytes
Fraction disease-free
Days post immunization

Figure 6

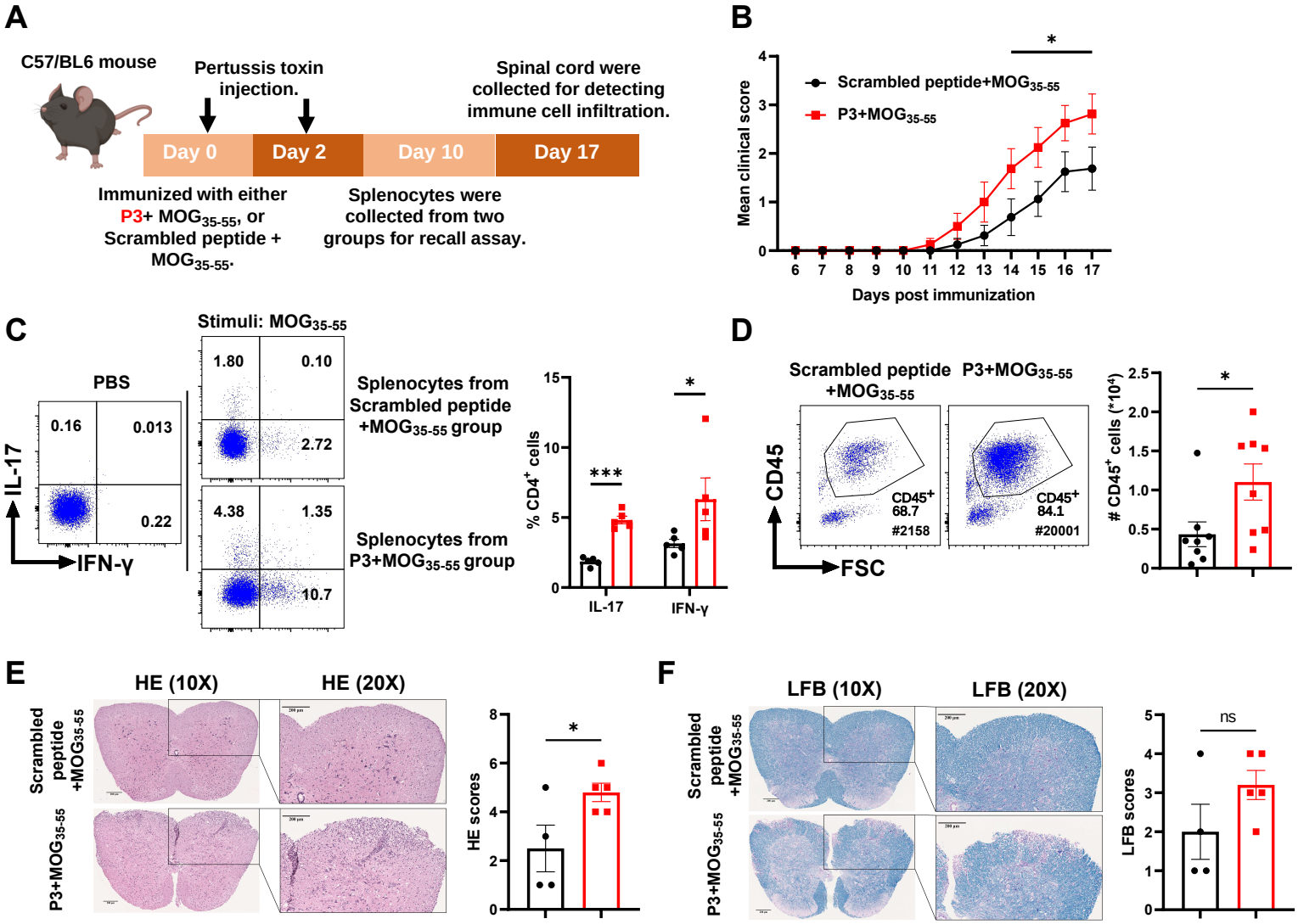
A
C57/BL6 mouse
Pertussis toxin injection.
Spinal cord were collected for detecting immune cell infiltration.
Day 0
Day 2
Day 10
Day 17
Immunized with either P3+ MOG35-55, or Scrambled peptide + MOG35-55.
Splenocytes were collected from two groups for recall assay.
B
Scrambled peptide+MOG35-55
P3+MOG35-55
Mean clinical score
Days post immunization
C
Stimuli: MOG35-55
PBS
IL-17
IFN-γ
0.16
0.013
0.22
1.80
0.10
2.72
4.38
1.35
10.7
Splenocytes from Scrambled peptide +MOG35-55 group
Splenocytes from P3+MOG35-55 group
% CD4+ cells
IL-17
IFN-γ
D
Scrambled peptide +MOG35-55
P3+MOG35-55
CD45
FSC
CD45+ 68.7 #2158
CD45+ 84.1 #20001
CD45+ cells (*10^4)
E
HE (10X)
HE (20X)
Scrambled peptide +MOG35-55
P3+MOG35-55
HE scores
F
LFB (10X)
LFB (20X)
Scrambled peptide +MOG35-55
P3+MOG35-55
LFB scores
ns

Figure 7

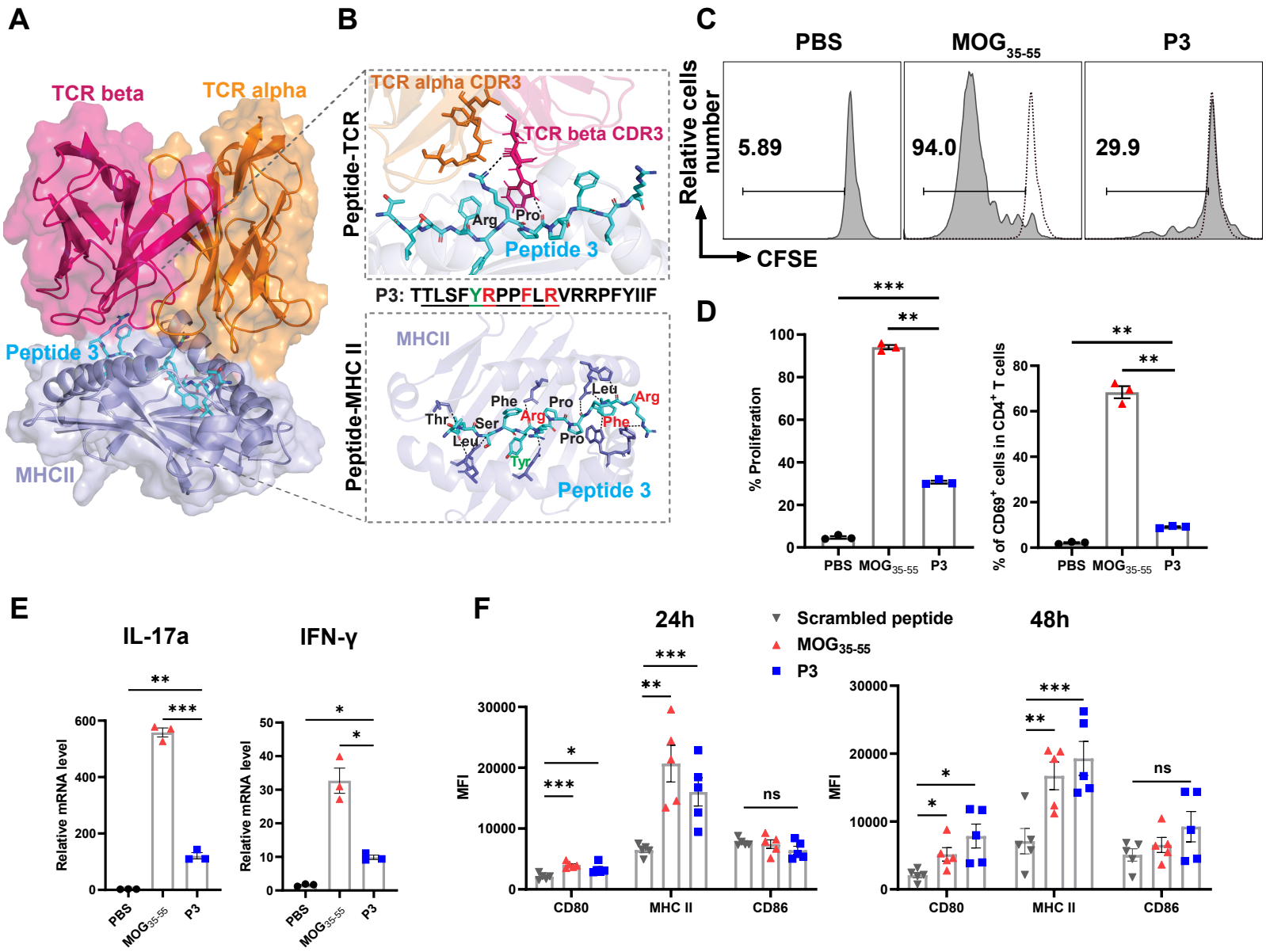
A
TCR beta
TCR alpha
Peptide 3
MHCII
B
Peptide-TCR
TCR alpha CDR3
TCR beta CDR3
Arg
Pro
Peptide 3
P3: TTLSFYRPPFLRVRRPFYIIF
Peptide-MHC II
MHCII
Phe
Pro
Leu
Arg
Thr
Ser
Arg
Phe
Leu
Pro
Tyr
Peptide 3
C
PBS
MOG35-55
P3
Relative cells number
5.89
94.0
29.9
CFSE
D
% Proliferation
% of CD69+ cells in CD4+ T cells
PBS
MOG35-55
P3
E
IL-17a
IFN-γ
Relative mRNA level
PBS
MOG35-55
P3
F
24h
48h
Scrambled peptide
MOG35-55
P3
MFI
CD80
MHC II
CD86
ns